Combustion and Flame 162 (2015) 1566–1574

Contents lists available at ScienceDirect

Combustion and Flame

journal homepage: www.elsevier.com/locate/combustflame

Dependence of sooting characteristics and temperature field of co-flow laminar pure and nitrogen-diluted ethylene–air diffusion flames on pressure

Ahmet E. Karataş, Ömer L. Gülder *

Institute for Aerospace Studies, University of Toronto, 4925 Dufferin Street, Toronto, Ontario M3H 5T6, Canada

ARTICLE INFO

Article history:
Received 2 April 2014
Received in revised form 15 November 2014
Accepted 16 November 2014
Available online 8 December 2014

Keywords:
Soot formation at high pressures
Ethylene diffusion flame
Pressure dependence of soot formation
Temperature of high-pressure diffusion flames

ABSTRACT

Pressure dependence of sooting characteristics and the flame temperature field of pure ethylene and ethylene diluted with nitrogen in co-flow laminar diffusion flames was investigated experimentally. The pressure range for ethylene was from atmospheric to 7 atm and to 20 atm for nitrogen-diluted ethylene flames. Spectrally-resolved line-of-sight soot radiation emission measurements were used to obtain radially resolved temperatures and soot volume fractions by using an Abel type inversion algorithm. A constant mass flow rate of ethylene was maintained at 0.48 mg/s at all pressures to match the carbon flow rates of gaseous alkane fuels experiments reported previously. Visible flame heights, as marked by the luminous soot radiation, initially increased with pressure, but changed little above 5 atm. Maximum local soot volume fraction of ethylene flames seems to scale with pressure raised to the third power (about 2.8). This is argued to be a relatively stronger pressure dependence of maximum soot volume fraction as compared to other gaseous fuels. A similarly higher pressure dependence was observed when the maximum soot yields of ethylene and other gaseous fuels were compared. It was shown that the soot yield dependence of ethylene flames does not conform to the unified dependence on pressure which was demonstrated for gaseous alkane fuels recently. The sooting propensity of nitrogen-diluted ethylene flames was shown to be less than that of *n*-heptane flames diluted with similar amount of nitrogen. Flame temperature profiles and averaged temperatures of ethylene flames showed similar characteristics as the other gaseous fuels, however radial temperature gradients in ethylene flames were much higher than those in gaseous alkane fuel flames.

1. Introduction

Soot aerosols exhausted into the atmosphere from air and land transportation engines constitute a significant portion of the particulate matter in the air. Soot aerosol, also called as black carbon, emitted to the atmosphere is not only an unwanted pollutant in the environment and is implicated in a number of health problems [1], but it also influences the thermal equilibrium of the planet. Deposition of soot aerosols on Polar Regions and the suspended soot particles in the atmosphere could be one of the major causes of the global warming originating from the human activity. Recent research efforts estimate the effect of soot on climate change to be second only to that of carbon dioxide, see for example [2].

Size limitations and fuel efficiency concerns dictate that most energy conversion devices based on combustion should operate at pressures much higher than atmospheric. Available soot research results reported recently for a limited number of fuels (mostly gaseous) have shown that the pressure is one the most significant parameters that influence soot formation [3]. A detailed description of the dependence of soot on pressure is not available and there is a lack of sound combustion and soot models that could be used for practical applications that operate at elevated pressures. For this reason, studies that would enhance our understanding of the effects of pressure on soot formation and oxidation are of great interest. Our current understanding of inception, growth, and oxidation of soot at pressures above atmospheric is quite limited, and tractable measurements at elevated pressures are needed to advance the field and provide a better understanding. The main objective of the current study is to investigate the effects of pressure on soot formation and temperature field in pure and nitrogen-diluted ethylene laminar diffusion flames at pressures above atmospheric, and compare the findings to similar measurements with gaseous and liquid alkane fuels. Ethylene is not a commercial

* Corresponding author. Fax: +1 416 667 7799.
E-mail address: ogulder@utias.utoronto.ca (Ö.L. Gülder).

http://dx.doi.org/10.1016/j.combustflame.2014.11.020
0010-2180/

fuel or an important component of commercial fuels used in combustion engines. However, in majority of research studies on soot processes ethylene has been used as the fuel, and some of the empirical models for soot processes have been based on and verified with measurements in ethylene flames. During the combustion of liquid hydrocarbons, ethylene is one of the most abundant olefins as an intermediate species. For studies related to soot, ethylene could be used to mimic the sooting properties of aviation kerosene as a simple surrogate.

One of the earlier studies of pure ethylene laminar diffusion flames on a co-flow burner was conducted by Flower and Bowman [4] at elevated pressures from atmospheric to 10 atm. Their main measurements were line-of-sight temperatures and integrated soot volume fractions along the flame centerline. Similar measurements were reported by McCrain and Roberts [5] conducted with a co-flow burner fueled by pure ethylene, and the pressure range was extended to 16 atm. Experiments of Lee and Na [6] with a similar configuration were done at pressures up to 4 atm. The experimental results reported by Darabkhani et al. [7] covered the same pressure range considered in [5] using a similar experimental rig. There are concerns related to the tractability of measurements in these studies with ethylene in laminar diffusion flames at elevated pressures. In studies reported in [4,5,7] the flames were non-smoking at pressures of atmospheric and a few atmospheres, meaning that the flames were burning below their smoke-point heights with less than smoke-point fuel mass flow rate. However, at pressures above a few atmospheres the fuel mass flow rates were no longer corresponding to non-smoking flames [4,5,7]. It is well-established that the smoke-point fuel mass flow rate varies strongly with pressure and decreases as the pressure is increased, as explained in detail in a recent review [3]. For high pressure soot experiments with laminar co-flow diffusion flames the fuel mass flow rate should be carefully selected. The fuel mass flow rate should be such that it should not exceed the smoke-point mass flow rate at the highest pressure of the experiment. This is essential for tractable soot measurements that are conducted for the purpose of assessing the effect of pressure on soot processes. Diluting the ethylene with an inert gas delays the onset of smoking [8] and allows a higher fuel mass flow rate to be used in the experiments, however the sooting behavior of pure ethylene is desirable as a reference bench-mark at elevated pressures. Further, it would be interesting to see whether the sooting characteristics of ethylene with pressure conform to the unified behavior of gaseous alkane fuels reported recently [9]. The only studies with pure ethylene in a tractable manner at elevated pressures were reported by Panek et al. [10] and Guo et al. [11] up to 5 and 8 atm, respectively, with an ethylene flow rate of 0.48 mg/s. Guo et al. [11] reported maximum soot volume fractions and integrated soot concentrations up to 8 atm; the temperature field within the flame envelope was not measured and soot yield information was not provided. Measurements reported in Panek et al. [10] have been repeated at 1, and 5 atm; and further measurements were done at 3 atm and at 7 atm with the same ethylene flow rate in the current work.

A series of tractable high pressure laminar flame soot studies has been reported by the senior author's group in recent years. Thomson et al. [12] and Joo and Gülder [13] studied methane laminar diffusion flames at pressures up to 40 atm and 60 atm, respectively. These were the first detailed data sets of radially resolved soot concentration and soot temperature measurements in laminar co-flow diffusion flames at elevated pressures. Measurements in propane diffusion flames using the same experimental setup as [13] were reported by Bento et al. [14]. Propane experiments were limited to the pressure range from atmospheric to 7.3 atm, and the measured soot and temperature profiles were comparable to those in [12] for the lower pressure range. The measurements were extended to ethane flames in [15] and the maximum pressure was 33 atm, and the results displayed similar behavior to that of methane flames although the soot concentration levels were much higher at similar pressures. Joo and Gülder [8] reported soot and temperature field measurements in nitrogen-diluted ethylene flames up to 35 atm [8]. Fuel to nitrogen mass ratio in diluted ethylene stream was 5 and this dilution ratio permitted to have non-smoking flames up to 35 atm. In a more recent report, it was shown that the high pressure soot yield data from laminar methane, ethane, and propane diffusion flames could be scaled, and the scaled maximum soot yields display a unified dependence on pressure [9]. Available experimental data show that the scaled maximum soot yield increases with pressure initially, but as the pressure further increases it reaches a plateau asymptotically, approximately at the critical pressure of the fuel [9]. First tractable measurements at elevated pressures with a liquid hydrocarbon were conducted in laminar diffusion flames of pre-vaporized *n*-heptane [16]. The fuel was diluted with a constant amount of nitrogen to have non-smoking flames up to 7 atm.

In the current study, the effects of pressure on sooting characteristics and temperature field of pure ethylene–air diffusion flames are studied. Further experiments were done with ethylene diluted with nitrogen for the purpose of comparison to similarly diluted *n*-heptane flames at pressures above atmospheric, reported by the current authors previously [16]. Results are compared to the characteristics of other gaseous and liquid fuels, and similarities and differences are discussed in terms of maximum soot volume fraction, soot yield, and temperature profiles within the flame envelope.

2. Experimental method

The experimental setup used in the current study is documented in detail previously, see for example [12–14,16]. Only a brief description, consisting of essential details, will be given here. The burner used is a circular co-flow laminar diffusion type burner which is commonly used in other similar studies [17]. Its inner diameter at the burner rim is 3 mm and the outer diameter decreases gradually to a tapered fine edge to prevent any recirculation zones forming. The material of the burner is stainless steel and the burner tube has an insert of metal porous material to help to minimize the flow non-uniformities. The co-flow air nozzle is about 25 mm in diameter, and the air channel is also fitted with porous material for the same purpose upstream of the burner exit.

The burner described above is mounted inside a high-pressure combustion chamber designed to be operated up to 110 atm pressure. Optical access to the chamber is provided through three optical quartz windows positioned at about the mid-height of the cylindrical chamber and are installed in the sidewall to provide line-of-sight and 90° scattering measurements. The internal diameter of the combustion chamber is about 240 mm whereas its height is 600 mm. The burner is fixed within the combustion chamber, and the chamber is mounted on an automated translation stage with vertical and horizontal movement capability so that the combustion chamber can be positioned as desired with respect to the stationary optical system for measurements.

The optical measurement technique is based on the analysis of spectral emission of radiation from the soot particles formed within the flame envelope. The original version of this technique has been known as two-color pyrometry, and the details of this refined method, known as soot spectral emission (SSE), is explained in detail by Snelling et al. [18]. Briefly, the flame is mapped point by point with a line-of-sight measurements of spectral radiation from 690 nm to 945 nm. Measurement resolution was 0.05 mm in horizontal direction (along the radius of the flame) whereas it was 0.5 mm in vertical direction. At each point at least 3 images of 1 s duration each were captured and both left and right sides of the

flame were scanned. The results correspond to the average of the right and left scans.

The radiation emission was imaged on a 1340 × 400 pixels CCD array, although only 1340 × 80 pixels were utilized for measurements. From a series of knife-edge scans, the horizontal spatial resolution was estimated as 0.07 mm, and the vertical resolution as 0.29 mm. The optical measurement system is frequently checked for intensity of radiation with a standard filament lamp whose calibration is traceable to National Institute for Standards and Technology (NIST). The line-of-sight radiation intensity measurements at a given height of the flame can be inverted through an Abel inversion algorithm to yield radially resolved intensities [19]. These radial emission intensities permit to infer profiles of temperature and soot concentration along the flame radius at a given height along the flame [18]. This process requires a knowledge of the soot optical properties, primarily complex soot refractive index. Since there seems to be no consensus on the correct value of the soot refractive index and its dependence on temperature and wavelength as well as on the history of the soot particles, we used in this work the same value we used in our previous publications for consistency [10–16,18]. The error committed as a result of the uncertainty in soot refractive index is discussed in the last part of the Section 3. Other details of the optical set up including the description of the spectrometer can be found in recent publications from this laboratory [13,16].

The mass flow rates of the ethylene, nitrogen and air supplied to the burner are measured by calibrated mass flow control units (Brooks). These flow controllers are frequently checked against a secondary standard flow meter (Sensidyne Gillabrator – 2) whose calibration is traceable to NIST. In order to deal with tractability of measurements at different pressures, fuel and air mass flow rates were kept constant at all pressures considered. The ethylene flow rate at all pressure levels was kept as 0.48 mg/s which corresponds to a carbon mass flow rate of 0.41 mg/s. This carbon flow rate is the same as the carbon flow rates in our previous work with other gaseous [12–15] and liquid fuels [16]. In nitrogen-diluted ethylene flame experiments, nitrogen flow rate was 0.96 mg/s, twice the ethylene mass flow rate. Ethylene and nitrogen flow rates are listed in Table 1. At all pressures, a constant co-flow air mass flow of 0.34 g/s is provided. This air mass flow rate is again similar to air flow rates used in our previous measurements.

3. Results and discussion

3.1. Visible flame shape

Still pictures of ethylene–air diffusion flames at pressures up to 9 atm are shown in Fig. 1a. The luminous flame height increased substantially from atmospheric pressure to 5 atm, but the rate of increase diminished towards 9 atm, suggesting that the flames are not fully buoyancy-dominated at 5 atm and below [20]. However, it was shown with similar flames that the flame height marked by the stoichiometric contour is almost constant with pressure to a first approximation [20,21]. The flame height at 9 atm is approximately 9 mm, slightly higher than the 8.4 mm predicted theoretically using the expressions proposed by Roper et al. [22]. For fully buoyancy-dominated flames, it is expected that the luminous flame heights are independent of pressure if the fuel

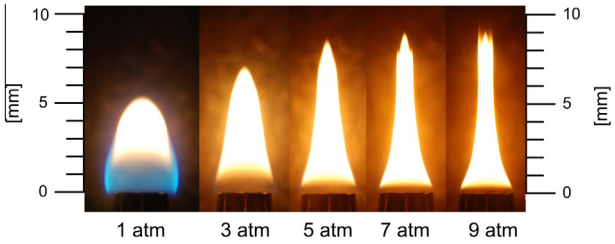

Fig. 1a. Still pictures of ethylene–air laminar diffusion flames from atmospheric pressure to 9 atm.

mass flow rate is fixed. For example, the experimental studies on sub- and super-atmospheric flames [8,10] show that the flame height increases with pressure at sub-atmospheric pressures but remains constant at elevated pressures above 10 atm. It should be noted that the centerline velocities of these flames from 1 atm to higher pressures do not change much with pressure [20], but the residence times increases, although in small amounts, up to 5 atm from 1 atm. This was argued to be due to the flames being not fully buoyancy-dominated up to 5 atm [20]. Simulations reported in [20] indicate that the residence time change from about 15 ms at 2 atm to about 19 ms at 5 atm for ethylene flames with the fuel mass flow rate used in this study.

Annular soot wings are apparent in the flame pictures corresponding to 5 and 7 atm, and the wing heights increase slightly with increasing pressure. The smoke point, defined as the condition when the visible tip of the soot wings exceeds the tip of the flame, was reached below 9 atm, and a lightly-smoking flame was established at 9 atm. With further pressure increase approaching 10 atm, the soot wings converged and transformed the flame into a heavily smoking flame along centreline (not shown).

Soot containing volume and its shape change noticeably with pressure, Fig. 1a. At atmospheric pressure, the luminous carbon zone is restricted to the tip of the flame, and it expands as the pressure is increased. The bulbous flame shape at atmospheric pressure transforms into an increasingly slimmer and inwardly curved flame shape with increasing pressure. All flames are attached to the burner within the pressure range studied, but the type of attachment zone is dependent on pressure. At atmospheric pressure, the flame is attached to the outer surface of the fuel tube below the fuel nozzle. At 3 atm, the attachment interface is relocated to the periphery of the fuel nozzle, and the blue zone, which is often associated with the triple flame structure, becomes less visible. Above 3 atm, the visible flame zone, thus the attachment interface, moves inwards towards the centreline and downwards towards the fuel nozzle.

Still pictures of ethylene flames diluted with nitrogen are shown in Fig. 1b. Overall features of the nitrogen-diluted flames are similar to previously reported high-pressure diffusion flame characteristics. The only distinction is that the flames seem to be fully buoyancy-dominated at all pressures, especially above 5 atm, yielding an almost constant visible flame height.

3.2. Soot volume fractions and yield

Two-dimensional contour plots of soot volume fractions and temperatures constructed from experimental measurements are shown in Fig. 2a for ethylene–air laminar diffusion flames at

Table 1
Mass flow rates of fuels and nitrogen. Data for *n*-heptane are from [16].

	Fuel mass flow rate (mg/s)	Fuel carbon flow rate (mg/s)	Nitrogen mass flow rate (mg/s)	Nitrogen to fuel mass ratio
Pure ethylene	0.48	0.41	0	
Diluted ethylene	0.48	0.41	0.96	2
Diluted *n*-heptane	0.49	0.41	1.04	2.12

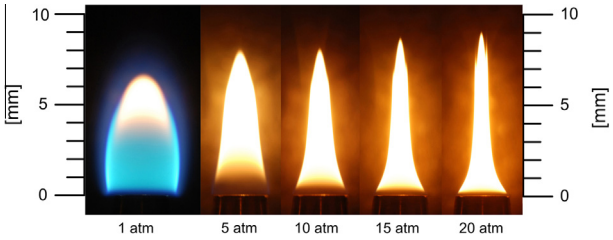

Fig. 1b. Still pictures of nitrogen-diluted ethylene–air laminar diffusion flames from atmospheric pressure to 20 atm.

pressures up to 7 atm, and in Fig. 2b for nitrogen-diluted ethylene flames at pressures up to 20 atm. The left hand sides of the plots are temperatures whereas the right hand sides depict soot volume fractions. It is noticeable that the temperature maps do not have smooth edges in Fig. 2, whereas the soot volume fraction contours are smoother. This is an artifact of the SSE measurement system which could measure only at locations where there is sufficient soot. Soot volume fractions gradually reduce to zero at the flame boundary, but temperatures encounter a sudden drop to co-flow air temperature from the relatively high values within the flame envelope. As a consequence of this, temperature values outside the flame envelope, where the temperature is expected to blend to the co-flow air temperature, are not available, hence the rugged edges. It is clear from the plots in Fig. 2 that soot volume fraction and temperature characteristics are affected significantly by pressure. Although an overall qualitative picture of soot concentration dependence on pressure emerges in Fig. 2, a detailed account of radial profiles of soot volume fractions are shown in Figs. 3–6 at 1, 3, 5, and 7 atm, respectively, at several heights above the burner (HAB) for pure ethylene fames.

As observed in atmospheric diffusion flames, soot first appears in an annular region just above the rim of the burner. This annular region gets closer to the burner rim and, to a certain extent, to the

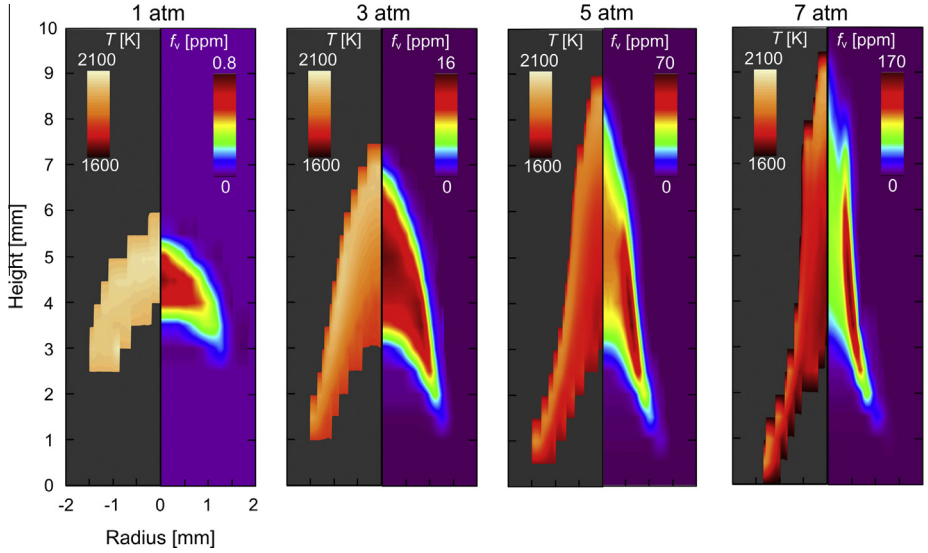

Fig. 2a. A two-dimensional representation of radially resolved soot volume fraction and temperature measurements in ethylene–air laminar diffusion flames from atmospheric pressure to 7 atm. The left and right hand sides of the flames in the contour graphs are temperature and soot volume fraction measurements, respectively.

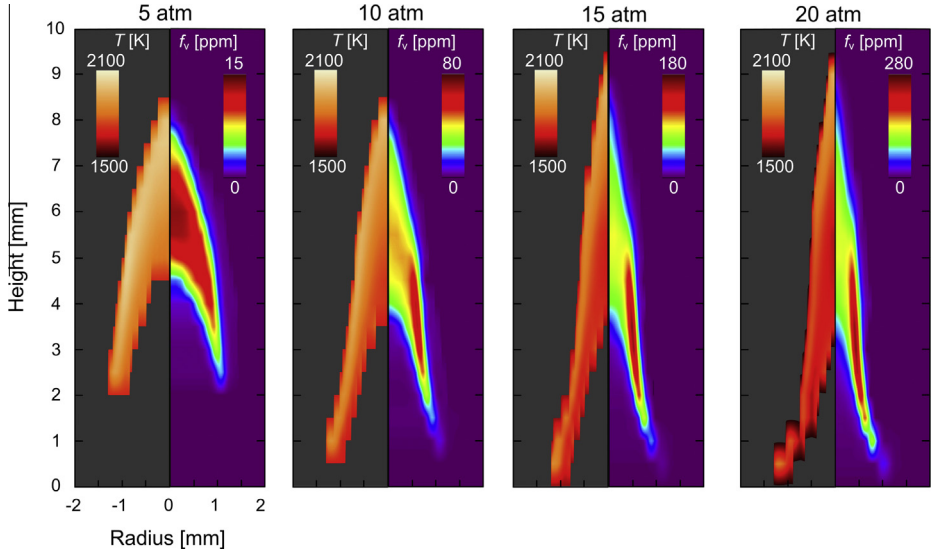

Fig. 2b. A two-dimensional representation of radially resolved soot volume fraction and temperature measurements in nitrogen-diluted ethylene–air laminar diffusion flames from 5 to 20 atm. The left and right hand sides of the flames in the contour graphs are temperature and soot volume fraction measurements, respectively.

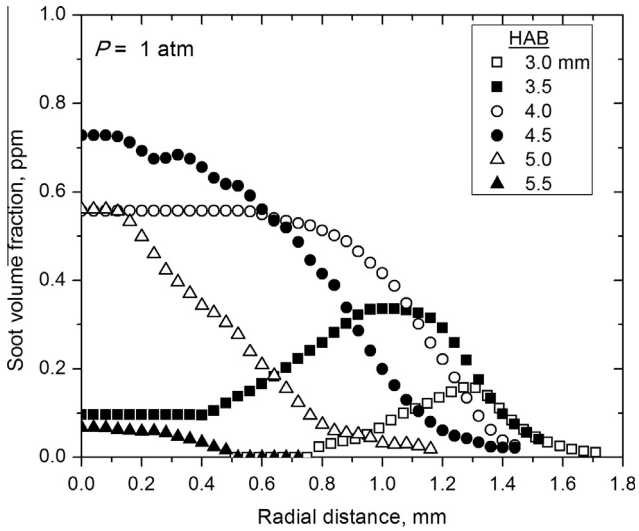

Fig. 3. Profiles of radial soot volume fractions at 1 atm at various heights above the burner.

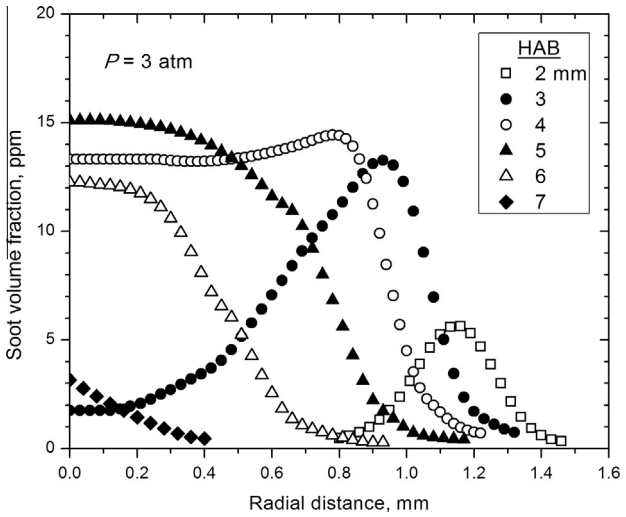

Fig. 4. Profiles of radial soot volume fractions at 3 atm at various heights above the burner.

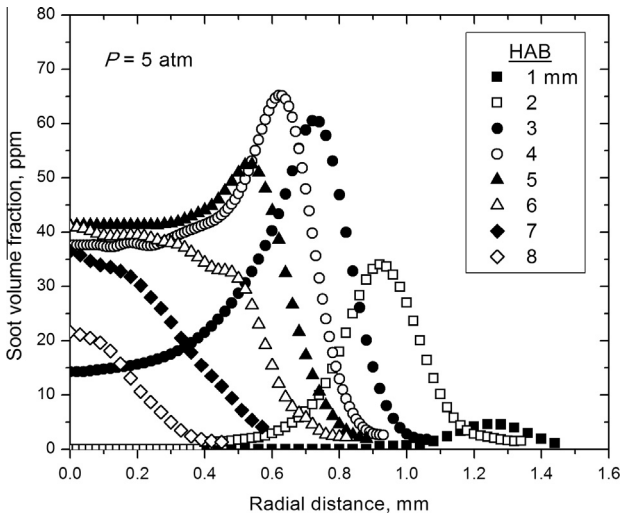

Fig. 5. Profiles of radial soot volume fractions at 5 atm at various heights above the burner.

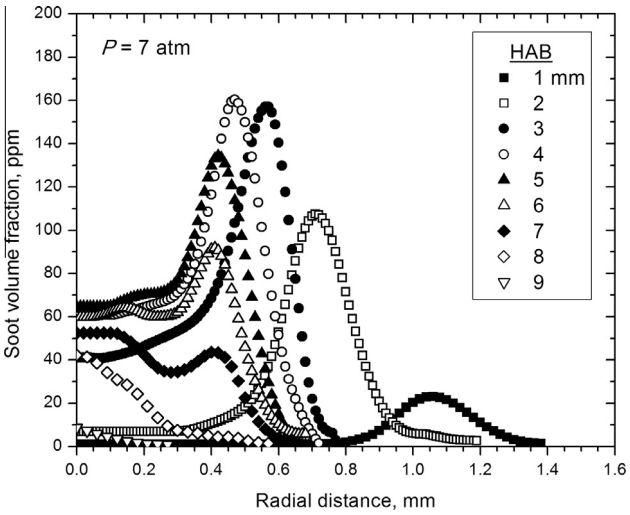

Fig. 6. Profiles of radial soot volume fractions at 7 atm at various heights above the burner.

flame centerline as pressure increases. Moving up from the flame base, soot zone expands towards the flame centerline such that the soot particles start appearing in the core of the flame. At the tip of the flame, soot volume fraction is maximum on the flame centerline, Figs. 3–6. The maximum soot volume fraction increases by two orders of magnitude from atmospheric pressure to 7 atm, that is, from less than 1 ppm at atmospheric pressure to almost 160 ppm at 7 atm, Figs. 3 and 6. As pressure increases the annular distribution of soot becomes more pronounced. The soot wings are successfully captured by the SSE measurement system shown as the annular crest at 7 atm in Fig. 2a.

Soot volume fraction results shown in Figs. 3 and 5 are generally similar to the data shown in Panek et al. [10] at 1 and 5 atm, respectively. However, there are some minor differences in 1 atm results between the two data sets (Fig. 3 as compared to Fig. 5 in Panek et al. [10]). This is most probably due to the relatively poor repeatability of the SSE system at lower soot concentrations.

The maximum local soot volume fractions from the current study are compared with previous measurements in ethylene flames [10,11] and in ethane [15] flames in Fig. 7. The fuel carbon mass flow rate is the same for all fuels. Agreement between the

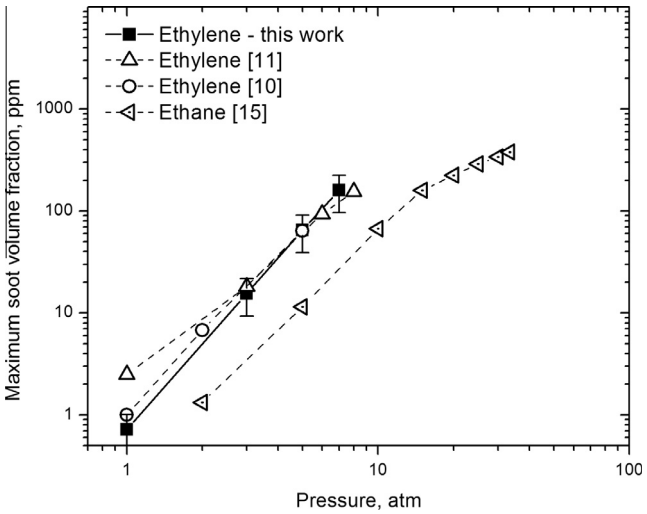

Fig. 7. Maximum local soot volume fractions measured in this work at 1, 3, 5, and 7 atm (denoted by full square symbols) compared to previous measurements with ethylene [10,11] as well as to ethane [15]. The fuel carbon mass flow rate is 0.41 mg/s for all fuels.

current results and previous measurements with ethylene is assuring, and the differences are well within the experimental uncertainties except for the atmospheric pressure, Fig. 7. Guo et al. [11] used a modified line-of-sight attenuation (diffused LOSA) to measure soot volume fractions whereas in the current work and in [10] SSE was used. It is known that at lower soot concentrations, LOSA is expected to be more accurate than SSE.

The slope of the line between 1 and 7 atm connecting the ethylene data points of the current work in Fig. 7 is about 2.8, implying that the pressure dependence of soot concentration in ethylene flames is stronger than other fuels for which data are available. However, if one takes into account the maximum soot volume fraction at 1 atm as reported in Guo et al. [11], the pressure sensitivity is about 2.6, still higher than the sensitivity of the other gaseous fuels within the same pressure range. It could be argued that maximum soot volume fraction is not exactly most relevant measure to assess the influence of pressure on soot in flames due to the compressibility of flame gases and incompressibility of solid soot particles. It was suggested that the soot yield, which is defined as the fraction of fuel's carbon turned into soot, is a better measure for assessing sensitivity to pressure [4]. The maximum soot yield then can be used to compare sooting sensitivities of different fuels to pressure in a tractable manner. To evaluate the soot yield of a flame, the carbon mass flow rate through a radial flame cross-section perpendicular to the flame axis can be calculated by using the following relationship

$$\dot{m}_s(z) = 2\pi\rho_s \int v_z(r,z) f_v(r,z) r dr \qquad (1)$$

In Eq. (1), $\rho_s = 1.8$ g/cm^3 is the soot density, v_z is the local axial velocity, f_v is the measured soot volume fraction, r is the radial coordinate along the flame radius, and z is the axial coordinate along the flame axis. In Roper's work, the flame acceleration constant a which is required to estimate the axial velocity from the relationship $v_z(z) = \sqrt{2az}$, is assumed as 25 m/s^2 at atmospheric pressure flames [22]. However, detailed numerical simulations of similar high pressure flames showed that this acceleration constant is about 32 m/s^2 [20,21]. Once the carbon mass flow rate is known, the soot yield can be evaluated by taking the ratio of it to the carbon mass flow rate at the nozzle exit within the fuel stream as $Y_s = \dot{m}_s/\dot{m}_c$, where $\dot{m}_c$ is the carbon mass flow rate at the nozzle exit. The results of this calculation for pure ethylene flames are shown in Fig. 8a. Axial location of the peak soot yield gets closer to the burner from 1 atm to 7 atm similar to previous observations in propane flames [14]. Slopes of the soot yield curves at lower axial locations within the flames increase significantly with increasing pressure. Soot yield profiles for nitrogen-diluted ethylene flames are shown in Fig. 8b at various pressures. Overall features are similar to pure ethylene flames and axial location of the peak soot yield seem to shift lower flame axial locations as the pressure is increased.

The maximum soot yields of pure ethylene, nitrogen-diluted ethylene, and nitrogen-diluted *n*-heptane flames are compared in Fig. 9. It should be noted that nitrogen-diluted *n*-heptane flame data are from Karataş et al. [16] reported from the senior author's laboratory recently. A surprising observation is that the sooting propensity of *n*-heptane is slightly higher than that of ethylene. Both fuels were diluted with nitrogen twice the mass flow rate of the fuel (in fact, *n*-heptane was diluted with about 8% more nitrogen than the ethylene flame [16]; see Table 1). Although this observation is at odds with the accepted belief that the soot propensity follows the order of alkanes < alkenes < alkynes < aromatics [23], this ordering of sooting propensity does not take molecular mass and the detailed chemical structure of the hydrocarbons into account [24,25]. To the authors' knowledge, no direct head-to-head comparison of atmospheric sooting propensities of *n*-heptane and ethylene is available in literature. But smoke point information for both fuels is available. Most recent smoke point height for ethylene has been reported as 88 mm [26] whereas for *n*-heptane it has been measured as 73 mm [27]. In addition, the correlation developed for liquid hydrocarbons yields a smoke point estimate for *n*-heptane as 60 mm [24]. The data at atmospheric pressure on sooting propensities of ethylene and *n*-heptane support the observations at elevated pressures with diluted fuels as depicted in Fig. 9.

The maximum soot yields of methane, ethane, and propane were shown recently to have similar sensitivity to pressure [9]. When the maximum soot yields of gaseous alkane fuels are scaled properly, they display unified pressure dependence [9]. The current ethylene soot yield results, obtained by using Eq. (1) above, are evaluated by the scaling procedure detailed in [9] and plotted in Fig. 10 along with the data of three gaseous alkane fuels. As observed with the maximum soot volume fraction variation with pressure in Fig. 7, ethylene's maximum soot yield displays a stronger dependence on pressure. To assess the statistical significance of the deviation of ethylene's response to pressure from those of

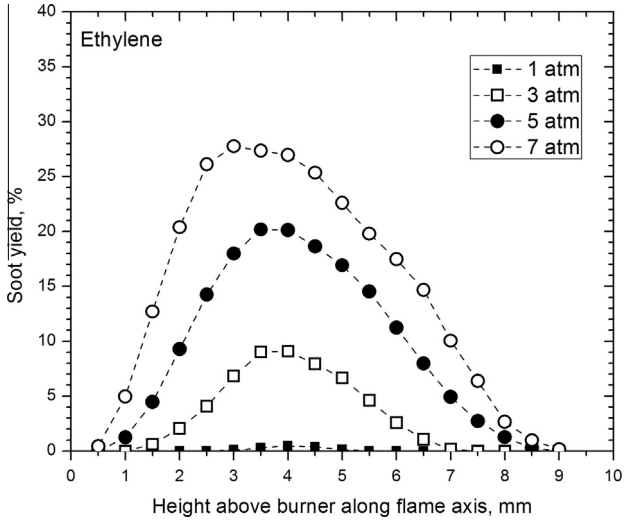

Fig. 8a. Soot yields of pure ethylene diffusion flames as a function of axial height above the burner at various pressures obtained using Eq. (1).

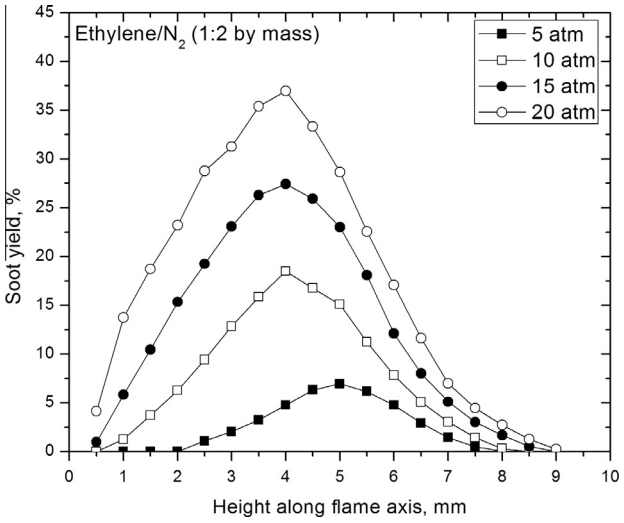

Fig. 8b. Soot yields of nitrogen-diluted ethylene diffusion flames as a function of axial height above the burner at various pressures obtained using Eq. (1).

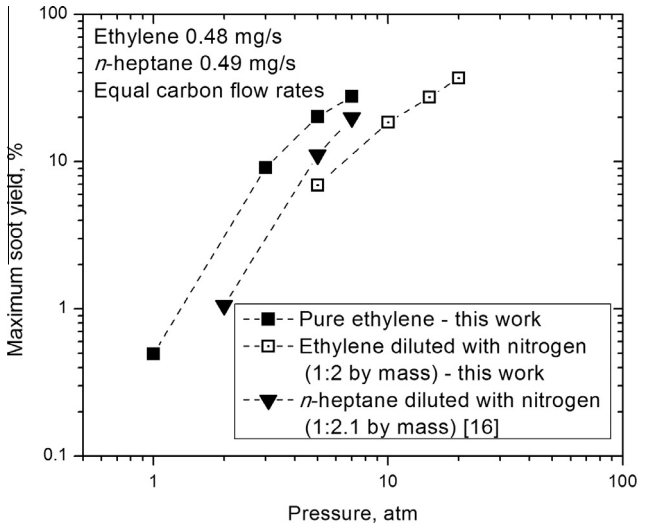

Fig. 9. Comparison of the maximum soot yields of pure ethylene, and nitrogen-diluted ethylene and *n*-heptane flames. Ethylene is diluted with 0.96 mg/s nitrogen, whereas *n*-heptane dilution was 1.04 mg/s nitrogen.

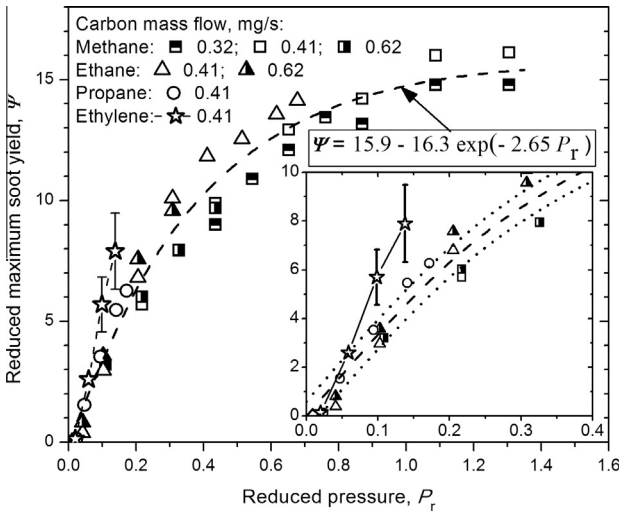

Fig. 10. Comparison of reduced maximum soot yields of ethylene diffusion flames as a function of reduced pressure to those of propane, ethane, and methane. Scaling methodologies for reduced soot yields and pressure are given in detail in [9]. The band between two short-dash curves in the inset designates the area of standard error of prediction of the empirical expression, which is a least square curve fit to the gaseous alkane fuel data [9].

other gaseous fuels, the standard error of prediction of the fitted curve proposed in [9] (expression shown in Fig. 10) was evaluated (which came about 0.6) and plotted as plus and minus standard error curves in the inset of Fig. 10. Clearly, the maximum soot yields of 5 and 7 atm flames are much higher than those of other fuels and fall outside the standard error band of predictions. The reason behind the observed behavior of ethylene's soot yield with pressure is not obvious and should be the subject of detailed numerical simulations to identify the responsible chemical (and physical) processes.

3.3. Temperature field

The local flame temperatures vary between 1600 and 2100 K in Fig. 2a. Atmospheric-pressure flame temperatures are around 2050 K with little spatial temperature variation within the flame. With increasing pressure, flame temperatures decrease, and the variation in local temperatures increases. Between 3 and 7 atm, local flame temperatures are less than the flame average at lower flame heights and towards the flame core. The oxidation of the soot particles within the upper half of the flame increases the local temperatures and the maximum temperatures are usually observed near the flame tip, Fig. 11. With increasing pressure, the flame experiences an increasing radiative heat loss as a consequence of higher soot concentrations. As a result overall flame temperatures drop as pressure increases, Fig. 12. Observed increase in soot concentration gradients at higher pressures lead to an increase in the temperature variation within the flame. Detailed temperature profiles at 7 atm are shown in Fig. 11 at several heights above the burner. The double peak in temperature profile at 7 mm height is a manifestation of the presence of soot wings at 7 atm. This is also seen in soot profiles at 6 and 7 mm heights in Fig. 6.

Averaged temperatures at 1, 3, 5, and 7 atm pressures from the line-of-sight emission measurements through the flame centerline as a function of height along flame axis are depicted in Fig. 12. These temperatures should correspond closely to peak soot volume fraction location temperatures [18], since the temperatures plotted in Fig. 12 represent a soot concentration-weighted average temperature along a chord through the flame centerline (perpendicular to the flame axis). An overall decrease in temperature as the pressure increases is clearly observed from these profiles. At 5 and 7 atm flames, a higher temperature region is observed close to

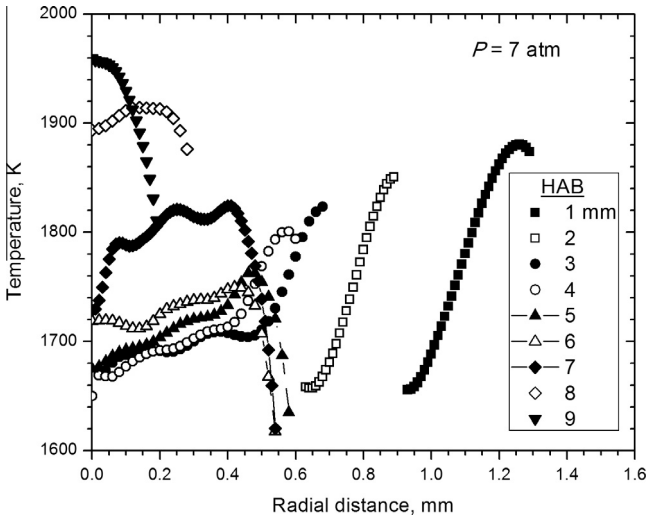

Fig. 11. Radial distributions of temperature at 7 atm at various heights above the burner.

the flame base similar to data reported in [15]. One of the reasons for this is the preheating of the reactants by the fuel nozzle, which is at a higher temperature as a result of heat transfer from the flame.

As the pressure increases, the luminous flame gets narrower, and this results in higher radial temperature gradients. Maximum radial temperature gradients, calculated from the temperature profiles, are shown in Fig. 13. The gradients are highest near the burner rim at lower pressures, however they are highest at 2 and 4 mm at higher pressures, and generally decrease with increasing height. Near the burner nozzle, radial temperature gradients are as high as 1400 K/mm at the higher pressures, whereas they drop to about zero near the tip of the flame, Fig. 13. These trends are similar to those observed in ethane flames [15], however, the radial temperature gradients are much higher in ethylene flames when compared at equal pressures. Comparison of the maximum radial temperature gradients of pure ethylene flames at 7 atm to those

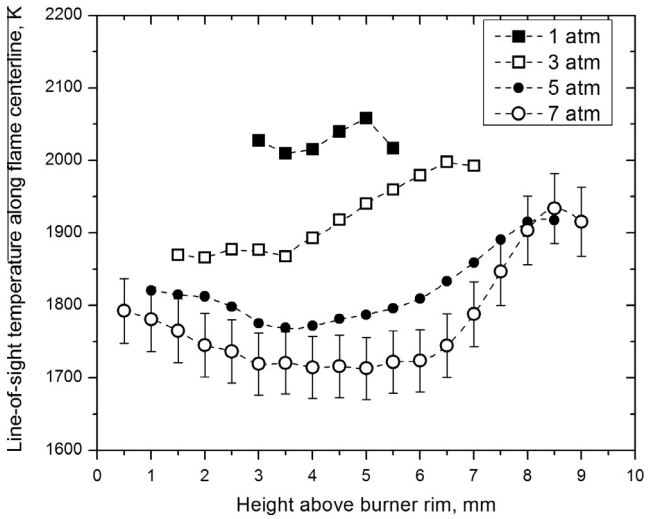

Fig. 12. Line-of-sight emission averaged soot temperature along the flame axis as a function of flame axial locations at various pressures.

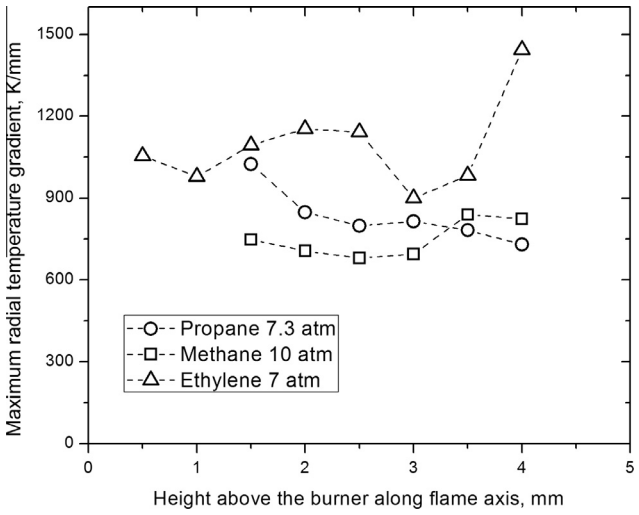

Fig. 14. Comparison of the maximum radial temperature gradients of pure ethylene flames at 7 atm to those of methane at 10 atm [8] and propane at 7.3 atm [14] at lower half of the flame where pyrolysis and soot formation are dominant.

of methane at 10 atm [8] and propane at 7.3 atm [14] at heights in the lower half of the flame where pyrolysis and soot formation are dominant is shown in Fig. 14. Although the pressures at which methane and propane flames were investigated are slightly higher than the ethylene pressure, temperature gradients in the ethylene flame is much higher than the other two flames. Higher radial temperature gradients near the burner exit at higher pressures mean that the thermal diffusion from the hot regions of the flame towards the flame centerline is enhanced. This causes higher fuel pyrolysis rates which lead to accelerated soot nucleation and growth as the pressure increases (see Fig. 14).

The flames investigated in this study are stabilized by the burner tube rim. As a result, significant heat transmission occurs between the flame and the burner tube that causes the temperature of the tube surface to increase. This heat transfer intensifies with increasing pressure as the flame base moves towards the burner rim and temperature gradients near the burner steepen. This is an unavoidable situation in the current experiments; however, its influence on soot formation and the flame structure can be assessed numerically. To account for gas-tube heat transfer, Charest et al. [20,21] prescribed a Robin-type boundary condition for the tube wall temperature. This boundary condition represents an arithmetic average between the two limits of a fixed temperature of 300 K and a zero-gradient condition [20,21].

Extensive data on radially-resolved soot concentrations and temperature profiles at various pressures for nitrogen-diluted flames are available in a thesis which has been completed recently by the lead author of this paper [28]. Limited data on nitrogen-diluted ethylene flames are presented in this paper to keep the paper concise.

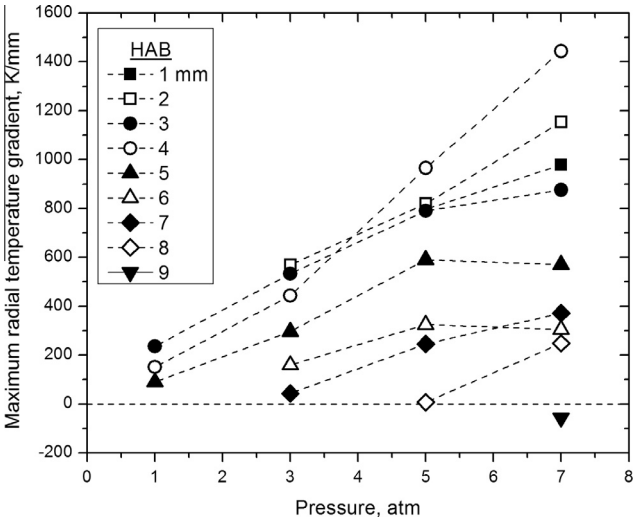

Fig. 13. Maximum radial gradients of soot temperature along the flame axis as a function of pressure at various flame axial locations.

3.4. Measurement uncertainties

When the soot volume fractions encountered in current flames reach a few hundred ppm levels, the first concern would be the uncertainty due to potential attenuation of radiation emission by soot. To assess the extent of self-attenuation of emissions a few detailed studies has been reported, see for example [18,29]. It is clear that the extent of self-attenuation could be judged by considering the optical thickness of the probe volume [29]. The optical thickness is proportional to the soot volume fraction and the path length through the soot containing zone. At the maximum pressure considered in this work, the soot volume fraction peaks at about 160 ppm at a height at which the path length is about 1.5 mm. This corresponds to an optical thickness of about 2 for a mid-wavelength of emission measurements and soot refractive index absorption function, $E(m)$, of 0.26. According to the detailed analysis presented in [29] for similar flames at pressure, the uncertainty introduced to soot volume fraction measurements by an optical thickness of 2 is still much smaller than the error due to the uncertainty in soot refractive index. On the other hand, the temperatures inferred from emission intensity measurements would be expected to be smaller by about 2% systematically [29].

The error introduced by the uncertainty in complex soot refractive index is the most significant source of systematic errors in these type of measurements. In spite of intensive efforts on quantifying the influence of temperature, wavelength and soot age on soot optical properties, no consensus has been reached in combustion literature as to the correct values [30–32]. As a result, in this work we assumed that the soot refractive index absorption function, $E(m)$, is constant as 0.26 to be consistent with our previous high-pressure soot volume fraction and temperature field

measurements with other fuels [12–16]. By using the approaches described in [12,18,29], the inferred maximum uncertainties in soot volume fraction and temperature measurements in this study are 40% and 5%, respectively. These values are comparable to uncertainties reported in similar measurements at elevated pressures.

4. Concluding remarks

In this paper the sensitivity of sooting characteristics and temperature field to pressure in co-flow laminar diffusion flames of pure ethylene–air from atmospheric pressure to 7 atm was studied experimentally. Also measured is the sooting propensity of ethylene diluted with nitrogen, up to a pressure of 20 atm. The line-of-sight soot spectral emission measurements were used to infer the radial distributions of temperature and soot volume fraction through an Abel inversion procedure. Ethylene mass flow rate was chosen to match the carbon flow rates of previously reported results with gaseous alkane fuels and maintained at 0.48 mg/s at all pressures. Luminous flame heights of pure ethylene flames, as marked by visible soot radiation, initially increased with pressure, but changed little above 5 atm. Nitrogen-diluted ethylene flames displayed fully buoyancy-dominated behavior at all pressures with constant visible flame heights. The results obtained indicate that, within the pressure range considered in this study, the maximum local soot volume fraction of pure ethylene flames seems to scale with pressure raised to the third power (about 2.8). This is a much higher pressure dependence of maximum soot volume fraction as compared to other gaseous fuels. To provide a more realistic comparison to other gaseous fuels, soot yield of the flames at various pressures were evaluated. A comparison of maximum soot yields of pure ethylene to other gaseous fuels at various pressures indicated that the pressure dependence of soot yield of ethylene flames is not similar to other gaseous fuels, and the sooting propensity of ethylene flames have a stronger dependence on pressure than gaseous alkane fuels. A comparison of the maximum soot yields of ethylene and *n*-heptane flames diluted with similar amounts of nitrogen indicates that sooting propensity of *n*-heptane is higher than that of ethylene. Flame temperature profiles and averaged temperatures of ethylene flames showed similar characteristics as other gaseous fuels, however radial temperature gradients in ethylene flames were much higher than those in gaseous alkane fuel flames for the same pressures.

Acknowledgments

Operational funds for this work have been provided by Natural Sciences and Engineering Research Council through Discovery and Strategic Project grants awarded to the senior author.

References

[1] L. Curtis, W. Rea, P. Smith-Willis, E. Fenyves, Y. Pan, Environ. Int. 32 (2006) 815–830.
[2] M.Z. Jacobson, Nature 409 (2006) 695–697.
[3] A.E. Karataş, Ö.L. Gülder, Prog. Energy Combust. Sci. 38 (2012) 818–845.
[4] W.L. Flower, C.T. Bowman, Proc. Combust. Inst. 21 (1988) 1115–1124.
[5] L.L. McCrain, W.L. Roberts, Combust. Flame 140 (2005) 60–69.
[6] W. Lee, Y.D. Na, JSME Int. J. Ser. B 43 (4) (2000) 550–555.
[7] H. Gohari Darabkhani, J. Bassi, H.W. Huang, Y. Zhang, Fuel 88 (2009) 264–271.
[8] H.I. Joo, Ö.L. Gülder, Combust. Flame 158 (2011) 416–422.
[9] Ö.L. Gülder, G. Intasopa, H.I. Joo, P.M. Mandatori, D.S. Bento, M.E. Vaillancourt, Combust. Flame 158 (2011) 2037–2044.
[10] N. Panek, M.R.J. Charest, Ö.L. Gülder, AIAA J. 50 (2012) 976–980.
[11] H. Guo, Z. Gu, K.A. Thomson, G.J. Smallwood, F.F. Baksh, Proc. Combust. Inst. 34 (2013) 1795–1802.
[12] K.A. Thomson, Ö.L. Gülder, E.J. Weckman, R.A. Fraser, G.J. Smallwood, D.R. Snelling, Combust. Flame 140 (2005) 222–232.
[13] H.I. Joo, Ö.L. Gülder, Proc. Combust. Inst. 32 (2009) 769–775.
[14] D.S. Bento, K.A. Thomson, Ö.L. Gülder, Combust. Flame 145 (2006) 765–778.
[15] P.M. Mandatori, Ö.L. Gülder, Proc. Combust. Inst. 33 (2011) 577–584.
[16] A.E. Karataş, G. Intasopa, Ö.L. Gülder, Combust. Flame 160 (2013) 1650–1656.
[17] I.M. Miller, H.G. Maahs, High-Pressure Flame System for Pollution Studies with Results for Methane–Air Diffusion Flames, NASA TN D-8407, 1977.
[18] D.R. Snelling, K.A. Thomson, G.J. Smallwood, Ö.L. Gülder, E.J. Weckman, R.A. Fraser, AIAA J. 40 (2002) 1789–1795.
[19] C.J. Dasch, Appl. Opt. 31 (1992) 1146–1152.
[20] M.R.J. Charest, C.P.T. Groth, Ö.L. Gülder, Combust. Flame 158 (2011) 1933–1945.
[21] M.R.J. Charest, C.P.T. Groth, Ö.L. Gülder, Combust. Flame 158 (2011) 860–875.
[22] F.G. Roper, C. Smith, A.C. Cunningham, Combust. Flame 29 (1977) 227–234.
[23] I. Glassman, R.E. Yetter, Combustion, fourth ed., 2008.
[24] Ö.L. Gülder, Combust. Flame 78 (1989) 179–194.
[25] N. Ladommatos, P. Rubenstein, P. Bennett, Fuel 75 (1996) 114–124.
[26] H. Guo, J.A. Castillo, P.B. Sunderland, Appl. Opt. 52 (33) (2013) 8040–8047.
[27] A.A. Akare, Investigating the links between smoke points, sooting thresholds, and particle number and size, M.Phil. Thesis, St. Edmund's College, Cambridge University, 2009 (available at <http://como.cheng.cam.ac.uk/dissertations/aax-MPhil.pdf> (accessed March 2014)).
[28] A.E. Karataş, High-pressure soot formation and diffusion flame extinction characteristics of gaseous and liquid fuels, PhD Thesis, University of Toronto, 2014. (available at <http://arrow.utias.utoronto.ca/~ogulder/karatasPhD2014.pdf>).
[29] F. Liu, K.A. Thomson, G.J. Smallwood, Combust. Flame 160 (2013) 1693–1705.
[30] S.C. Li, C.L. Tien, Proc. Combust. Inst. 18 (1981) 1159–1166.
[31] T.T. Charalampopoulos, H. Chang, B. Stagg, Fuel 68 (1989) 1173–1179.
[32] S.S. Krishnan, K.-C. Lin, G.M. Faeth, J. Heat Transfer 122 (2000) 517–524.